One-pot Surfactant-free Modulation of Size and Functional Group Distribution in Thermoresponsive Microgels

Apostolos A. Karanastasis[†*], Gopal S. Kenath[†], Dustin Andersen[†], Demosthenes Fokas[§], Chang Y. Ryu[‡], Chaitanya K. Ullal[†]

† Department of Materials Science and Engineering, Rensselaer Polytechnic Institute, Troy, New York, USA

§ Department of Materials Science and Engineering, University of Ioannina, Ioannina, Greece

‡ Department of Chemistry and Chemical Biology, Rensselaer Polytechnic Institute, Troy, New York, USA

Abstract. Control over the size and functional group distribution of soft responsive hydrogel particles is essential for applications such as drug delivery, catalysis and chemical sensing. Traditionally, targeted functional group distributions are achieved with semi-batch techniques which require specialized equipment, while the preparation of size-tailored particles typically involves the use of surfactants. Herein, we present a simple and robust surfactant-free method for the modulation of size and carboxylic acid functional group distribution in poly(N-isopropylacrylamide) thermoresponsive microgels, employing reaction pH as the single experimental parameter. The varying distributions of carboxylic acid residues arise due to differences in kinetic reactivity, which are a function of the degree of dissociation of methacrylic acid, and thus of reaction pH. Incorporated charged residues induce a surfactant-like action during the particle nucleation stage, and impact the final particle size. Characterization with dynamic light scattering, and electron microscopy consistently supports the pH-tailored morphology of the microgels. A mathematical model which accounts for particle deformation on the imaging substrate also shows excellent agreement with the experimental results.

Keywords: microgels; responsive colloids; pNiPAm; functional group distribution; one-pot; surfactant-free

Graphical Abstract

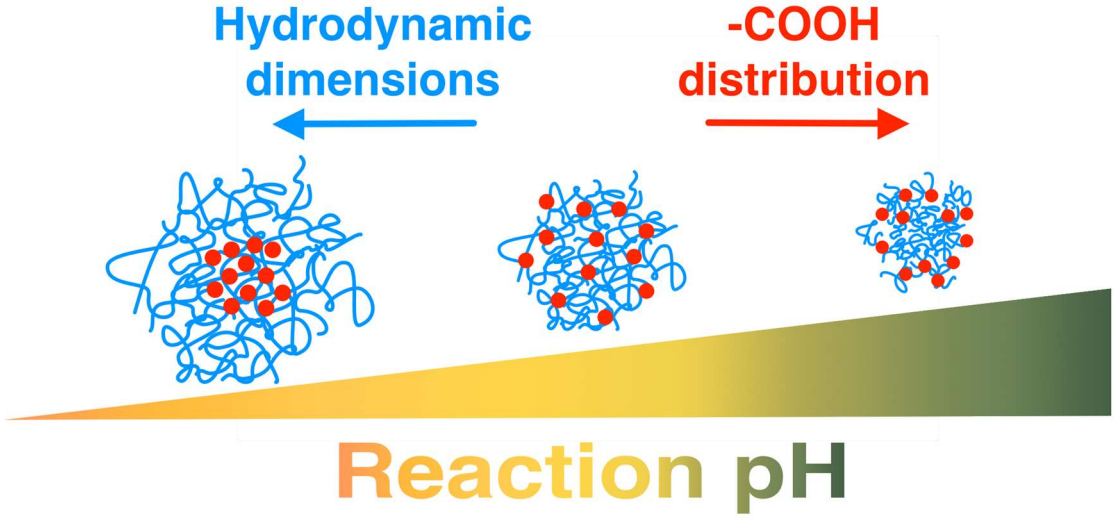

Introduction

Soft thermoresponsive colloidal gel particles, or microgels, have evolved into a distinct class of polymeric materials that hold promise for contemporary applications in fields such as biocatalysis [1][2], chemical sensing [3][4], emulsification [5], soft actuation [6] and drug delivery [7][8]. Although a multitude of monomers have been explored as the thermoresponsive component, microgel systems based on the well-studied thermoresponsive polymer poly(*N*-isopropylacrylamide) (PNiPAm) continue to draw the attention of the scientific community [9][10]. PNiPAm-based microgels adopt a highly hydrated swollen state at room temperature [11], while heating above the lower critical solution temperature (LCST) of ~32 °C causes the contraction of the colloid and the expulsion of a significant portion of the aqueous fraction [12]. This volumetric phase transition (VPT) is fast and reversible.

The common denominator of multifunctional PNiPAm-based microgel systems is the co-existence of the thermoresponsive backbone with monomeric residues of some functional group(s), which either endow environmental responsiveness (pH [13], light [14][15], glucose [16]) or serve as sites for subsequent chemical functionalization. Moreover, the distribution of the functional groups inside the thermoresponsive matrix is associated with the fine-tuning of properties, as exemplified in a drug delivery microgel platform where the carboxylic acid group topology was directly correlated with the binding capacity of various drugs [17]. Another important design parameter of microgel systems is the tailoring of hydrodynamic dimensions, as highlighted in a diverse set of applications that span from nano-pattering [18], to injectable drug administration [19] and selective protein adsorption [20].

Contributions that control the distribution of carboxylic acid species in thermoresponsive microgels can be found in the literature; Pelton and Hoare [21] provide a comprehensive review on the subject. In essence, it has been demonstrated that for microgels synthesized commonly via precipitation polymerization, charge distribution inhomogeneities within PNiPAm microgels arise as a consequence of differences in kinetic reactivity between the polymerizable acids and NiPAm, the main monomer. In order to circumvent the kinetic reactivity mismatch in the NiPAm-methacrylic acid (MAAc) system and prepare particles with custom charge distributions, the Hoare group employed a semi-batch strategy where MAAc was added to the reaction at various feeding rates [22]. Equivalent results for the same system have been reported by Ngai et al. [23] adopting a delayed feeding approach.

Interestingly, pH is an overlooked synthetic parameter in precipitation polymerization; when ionizable monomers such as MAAc are introduced, reaction pH is simply determined by their relative concentration [24]. To the best of our knowledge, regulation of reaction pH has not been reported in microgel synthesis. Separately, pH adjustment has been explored as a handle for the manipulation of the

compositional drift in linear polymers. Rintoul and Wandrey [25] studied the dependence of relative reactivities on pH for the acrylamide (AA) - acrylic acid (AAc) system. A preference for homopropagation of AAc was found at acidic pH, with a gradual reversal of the trend for increasing pH. Lacik *et al.* [26] reported on the decrease of one order of magnitude of the propagation constant, k_p, of MAAc when it shifted from the uncharged to the negatively charged state. Dubey *et al.* [27] tuned the degree of MAAc ionization for the synthesis of linear polyampholytes with targeted comonomer compositions.

In light of recent results, which have proved that precipitation polymerization follows free-radical solution polymerization kinetics [28], and separately, that the spatial distribution of residues are a strong function of the respective propagation kinetics [29][30][31], we hypothesized that the pH-mediated regulation of monomeric residue distribution within the linear chain during the reaction, will be reflected volumetrically at the particles. Further motivation was provided by work from the Lyon group, where homogeneously crosslinked particles were prepared via precipitation polymerization by matching the relative reactivities of the monomer and the crosslinker [32]. In the present work, we demonstrate that adjustment of reaction pH in precipitation polymerization results in the modulation of size and charge distribution within P(NiPAm-*co*-MAAc) microgels. We present results for three reaction pH conditions corresponding to the fully protonated (pH=3.04), partially dissociated (pH=5.05) and fully deprotonated (pH=7.38) states of the monomer. We report a tailoring of the charge distribution and a concomitant modulation in particle size from ~700 nm down to ~200 nm. A mechanism of surfactant-like action of the charged residues is introduced for the interpretation of the recorded size variation.

Experimental

Materials. *N*-isopropylacrylamide (NiPAm) (Sigma, 97%) was recrystallized twice from hexane before use. *N,N′*-Methylenebisacrylamide (BIS) (Sigma, 99%), methacrylic acid (MAAc) (Sigma, 99%), sodium dodecyl sulphate (SDS) (Sigma, 99%) and potassium persulfate (KPS) (Acros Organics, 99+%) were used as received. Standard reagent grade NaOH, HCl (1M), sodium carbonate, sodium bicarbonate, sodium citrate and citric acid were used for the preparation of buffers and stock solutions. HPLC grade H_2O (Fisher Chemical) was used throughout the experiments. Formvar coated grids (200-mesh, Cu) were purchased from Ted Pella (USA). Uranyl acetate (2% solution, Electron Microscopy Sciences) was used to prepare dilute staining solutions.

Synthesis and Purification. Aqueous monomer stock solutions at prescribed concentrations (24.25 mg/ml NiPAm, 6.17 mg/ml BIS and 3.44 mg/ml MAAc) were prepared. Aliquots were drawn from the stocks (7 ml NiPAm, 1.5 ml BIS and 1.5 ml MAAc), combined into 20 ml borosilicate scintillation vials and the reaction pH (3.04, 5.05 and 7.38) adjusted by manual titration under mild stirring. Specifically, microliter volumes (10-100 ul) of HCl/NaOH solutions with concentrations ranging from 0.001- 0.1M and pure H_2O were added in stepwise fashion while the pH was monitored in real time. This procedure was iterated up to the final reaction volume (12 ml). Sample tagging follows reaction pH conditions, e.g. S304 was synthesized at pH=3.04 etc. The reaction pH was adjusted with sole addition of acidic or basic solution and pure H_2O in order to maintain the ionic strength of the reaction medium at a minimum; there was no addition of basic solution when regulating the pH of the S304 run. The reaction vials were then degassed in parallel for 30 min (SI Photo 1) and placed into a water bath at 70 °C for another 30 min, after which the reactions were sequentially initiated by injection of 100 ul of a 30 mg/ml KPS solution under an Ar blanket. Each reaction was sparged with Ar for 20 sec in order to ensure homogeneous dissolution of the initiator, and was left to polymerize for 60 min. The reactions were quenched by immersion of the vials into ice-water. 4 ml of the crude dispersions were added into 3 dram borosilicate glass vials containing 100 µl 0.1 M NaOH and left to stir for 24 h. The samples were subjected to 2 cycles of ultracentrifugation at 40k RPM for 60 min, reconstituted with 2 ml H_2O, lyophilized and stored at 4 °C for future use. The same protocol was employed for the preparation of control samples by replacing the amount of MAAc solution with H_2O.

Instruments and Methods. A Mettler Toledo MP220 pH-meter equipped with an LE407 glass electrode was used for monitoring pH. Characterization of particle size was performed with an Anton Paar Litesizer 500 instrument operating at 90° geometry. Freeze dried samples were re-dispersed at a target concentration of 0.1% w/v using citrate (pH = 4) or carbonate (pH = 9) buffers. Samples prepared at pH=5.05 and pH=7.38 were additionally measured in citrate buffer with SDS at 0.82 mM. Samples were equilibrated for 15 min prior to each size measurement of the temperature sweeps. Data analysis was performed with the Anton-Paar Kalliope software. Polydispersity index (PDI) information is encoded in the hydrodynamic diameter versus temperature graphs (D_h vs T) as error bars with $\sigma = \pm (D_h \times PDI)/2$. The error bar is comparable to the marker size when not discernible. Transmission Electron Microscopy (TEM) was performed with a JEOL JEM 2011 instrument. Sample preparation for the TEM study was done following a previously reported protocol by Hoare *et al.* [22]. The TEM samples, which were cast on Formvar coated grids, were also examined with Scanning Electron Microscopy (SEM) using an FEI Versa 3D instrument.

Construction of the model: The deformed morphology of the microgels in the collapsed state, exhibiting core (S304), uniform (S505) and shell topologies (S738), are modeled as semi-spheroids with the minor axis along the z direction and the two equal major axes along the x and y directions. For the core topology, the -COOH distribution is modeled as an elliptical sigmoid, Eqn 1., with a large plateau. A gaussian is convolved with the distribution to introduce a diffuse interface at the boundary of the stained core and unstained shell. The extent of the core in x and y is determined by the radial distribution profile in the TEM micrographs. The same cutoff percentage value was used for the z axis. The uniform topology is modeled by an elliptical sigmoidal function that extends throughout the dimensions of the microgel. Finally, for the shell topology, the elliptical sigmoid was used to describe the distribution within the shell. The distribution is set to zero for radial values below an inner boundary, which is also defined by an ellipse. The inner ellipse is assigned a different eccentricity than the outer boundary in order to capture the non-uniform deformation induced by drying on the substrate. The inner boundary is convolved with a Gaussian function to represent a diffuse interface between the stained shell and unstained core. The SI lists the values of the parameters used to model each topology.

$$f(x,z) = Base - \frac{Max}{1+\frac{(r_0-r)}{Rate}} \quad (1)$$

where $r = \sqrt{\frac{x^2}{a^2} + \frac{z^2}{b^2}}$.

Results and Discussion

Microgel Synthesis and Purification. Non-stirred precipitation polymerization [28] is a recent method for the synthesis of pristine PNiPAm microgels. In our hands, it proved to be robust and reproducible for the parallelized preparation of p(NiPAm-*co*-MAAc) particles at variable pH conditions. Liquid handling of monomers from solution stocks and exclusion of paddled stirring mitigated sources of potential experimental error. In all tested reaction pHs, the crude final dispersions were colloidally stable, below and above the VPTT, implying the presence of an efficient stabilization mechanism during precipitation polymerization in the surfactant-free conditions. The samples were thoroughly stirred at alkaline conditions prior to purification with ultracentrifugation in order to effectively remove any physisorbed sol from the particles.

Microgel Size. Irrespective of the carboxylic acid topology (core-localized, homogeneously distributed or shell-localized), the p(NiPAm-co-MAAc) microgel system traverses from the non-ionized to the fully ionized state within the pH range of 5 to 7 [22],[23]. In both pH=4 and pH=9 testing conditions, an opposite trend between size and reaction basicity is observed (Table 1); higher degrees of ionization of

the MAAc monomer during the reaction led to smaller particle size. Control runs at similar reaction pHs and in the absence of MAAc indicated no such trend in the variation of size (SI Figure 1). The recorded differences in size could thus be ascribed to the effect of pH on the decomposition kinetics of KPS at 70 °C and the varying effect of Cl^- or Na^+ counterions on the colloidal stability of primary nuclei.

Table 1. Summary of selected physical properties of microgel samples measured at the pHs indicated.

	Swollen D_h (nm)		Colloidal Stability above LCST		VPTT (°C)	
	Testing pH=4	**Testing pH=9**	**Testing pH=4**	**Testing pH=9**	**Testing pH=4**	**Testing pH=9**
S304	706 ± 8	670 ± 41	Yes	Yes	~ 30	N/A (two-step)
S505	396 ± 23	420 ± 2	No	Yes	~ 32.5	N/A (pseudo-linear)
S738	190 ± 6	193 ± 4	No	Yes	~ 32.5	~ 32.5

Deswelling Profiles and Morphological Basis. Temperature varying DLS at two different states, corresponding to the fully protonated (pH = 4) and fully deprotonated (pH = 9) forms of MAAc residues within the microgels, was employed to investigate the thermal behavior of the microgels, and infer the COOH distributions. The synthesis of microgels with MAAc in a batch reaction where pH was not intentionally controlled has been established to result in the COOH being concentrated in the core of the resultant microgel [22],[23]. These conditions correspond to a pH of ~3.5. The thermal transition profiles of S304, in which the reaction pH is intentionally set to 3.04, are consistent with the established conclusion that at these pHs, the higher k_p of the MAAc results in the MAAc being localized at the microgel core. At pH=9, a two-step deswelling profile is evident (Figure 1, green curve). Such multistep profiles have been reported in the literature for pNiPAm-carboxylic acid copolymer microgels, including for microgels with COOH localized in the core [33],[13],[34],[35]. We hypothesize these deswelling profiles reflect an interplay between attractive polymer-polymer interactions and electrostatic repulsions induced in the collapsing network by ionized MAAc residues. Presumably, these antagonistic interactions shift the VPT of the core region to a higher temperature than the native LCST of PNiPAm (~ 31 °C). On the other hand, chains near the periphery are subjected primarily to attractive hydrophobic interactions as well as comparatively minor repulsion from sulphate groups; thus, as the sample is heated, these chains collapse at a lower temperature (Figure 1, Panel A).

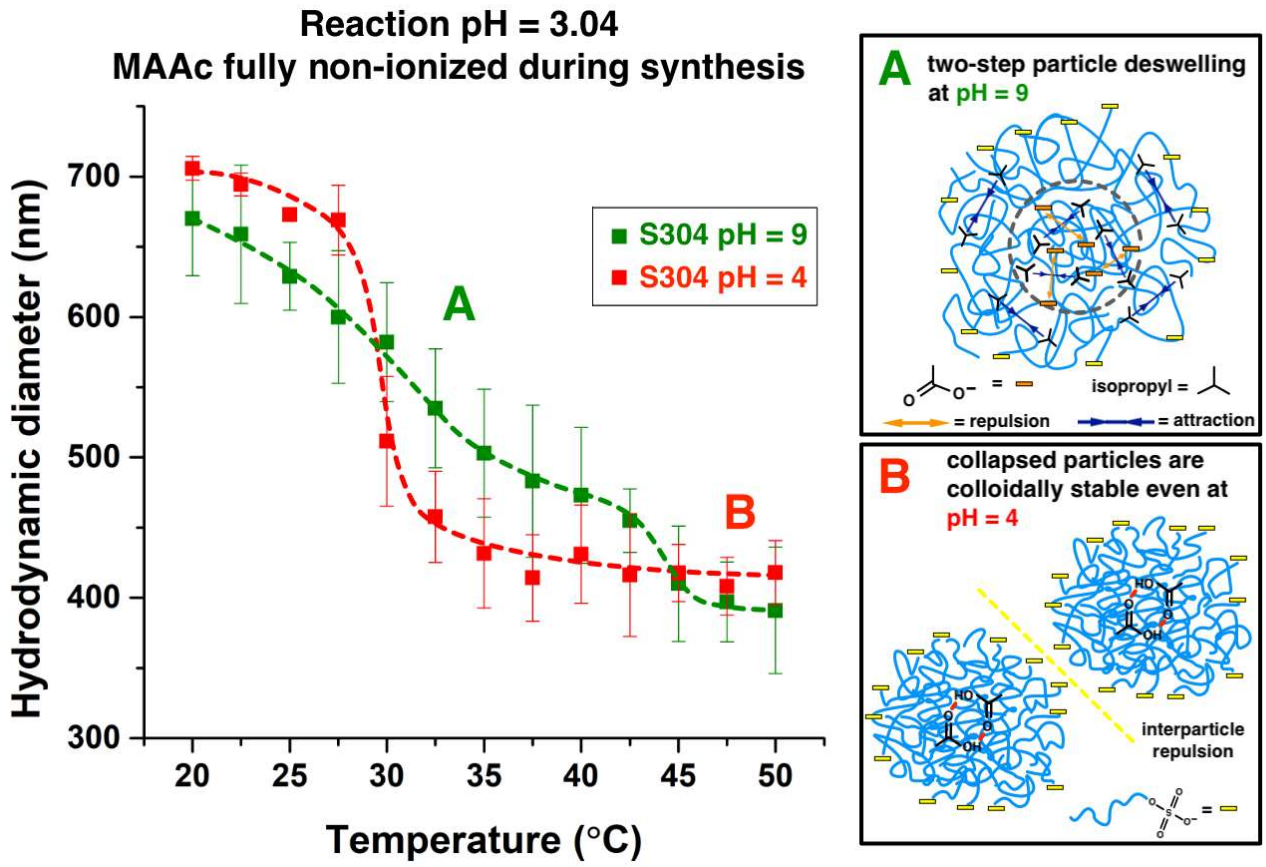

Figure 1. D_h versus T profiles for S304 at pH=4 and pH=9. Dashed lines are visual aids. Panel A: at pH=4 the presence of protonated -COOH residues at the particle core leads to H-bonding intra-particle interactions. Particles remain stable above the pNiPAm LCST due to inter-particle repulsive interactions stemming from residual initiator charged groups with very low pK_a. Panel B: at pH=9, the two-step deswelling profile is indicative of regions with distinct VPTTs. The particle core is rich in ionized -COO^- groups which hinder the collapse of the network. Network chains near the periphery are subjected primarily to attractive hydrophobic interactions and collapse at lower temperatures compared to the core.

This picture is contrasted with the thermal response at pH = 4, where the VPT is suppressed to a lower temperature than the LCST of PNiPAm. Such a phenomena is not unexpected as it is known that weak polyacids are known to form hydrogen bonds among the acid units and even with NIPAM [34],[36]. Thus, the fully protonated MAAc residues at the core (Figure 1, Panel B) favor polymer-polymer interactions by the combined effect of reduced hydrophilicity and hydrogen bonding between protonated segments. It is noteworthy that S304, in contrast to S505 and S738, remained colloidally stable at pH=4. This behavior can be ascribed to the presence of KPS charged fragments throughout the volume of all the particles, which, only in the case of the low pH where methacrylic acid is not present at the surface, provides stabilization of the particles [37],[38]. The inference of the carboxylic acid topology by DLS given above is purely phenomenological, and albeit analogous explanations have been reported for the

pNiPAm-co-AAc (AAc: acrylic acid) system [34], we substantiated these results only after the combined study with SEM/TEM and modeling, as it will be discussed below.

The deswelling profile of S505 (intermediate degree of MAAc dissociation during polymerization) at pH=9 testing conditions lacks a clear VPTT, albeit in this case multistep deswelling cannot be identified. We characterize this profile as quasi-linear and we hypothesize that it stems from a uniform distribution of carboxylic acid residues (Figure 2, Panel A). A similar thermal response in a pNiPAm-based microgel system, also arising from competitive interactions, has been reported by Zeiser *et al.* [39]; an innate osmotic term drives particle swelling below LCST while a strain term favors particle collapse.

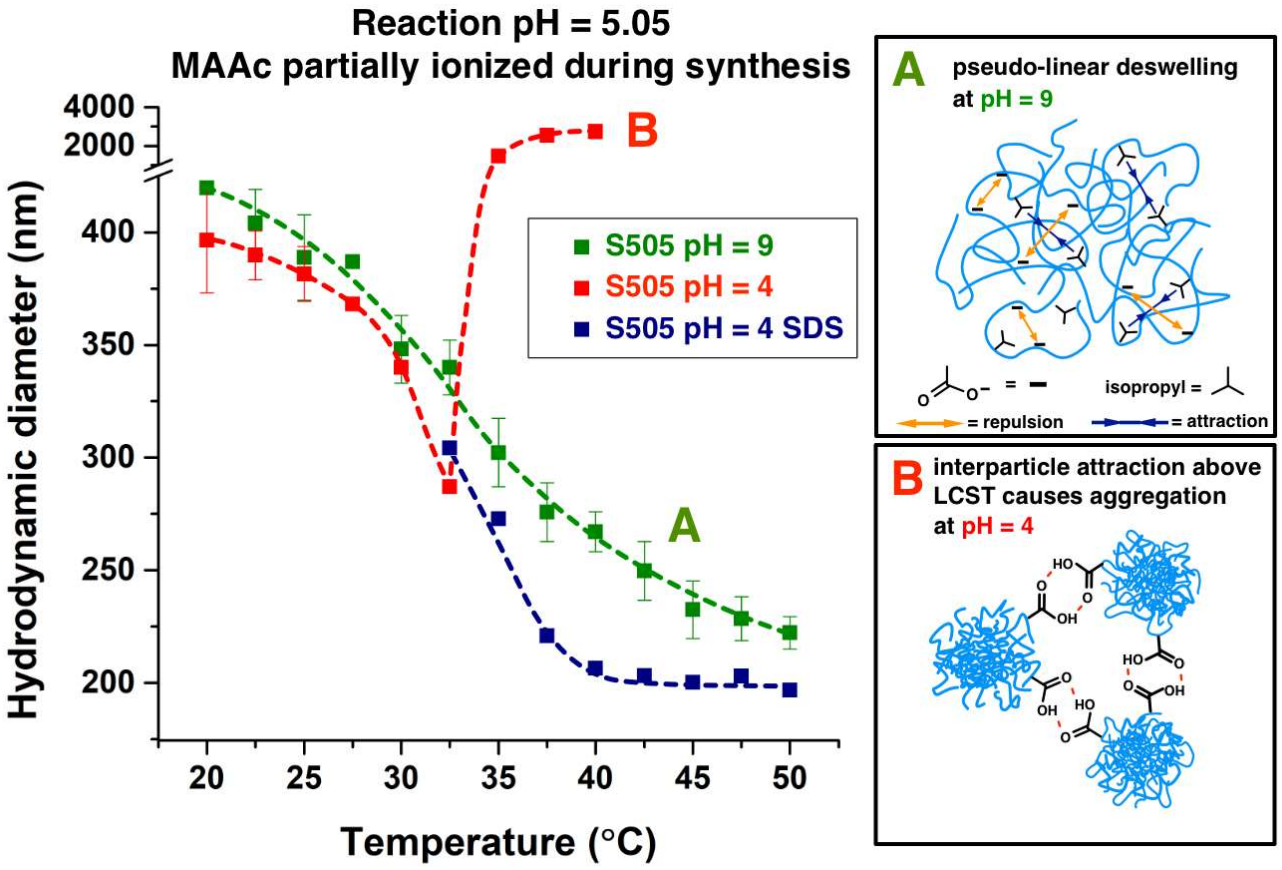

Figure 2. D_h versus T profiles for S505 at pH=4 and pH=9. Dashed lines are visual aids. Panel A: at pH=4 the presence of protonated -COOH residues at the particle surface leads to H-bonding inter-particle interactions and particles are unstable above the pNiPAm LCST. Panel B: at pH=9, a quasi-linear deswelling profile, characteristic of a uniform distribution of charged groups and the gradual deswelling as a result of the balance between opposing terms.

Strikingly, at pH=4 testing conditions and above 32.5 °C, S505 formed micron sized aggregates, indicating that interparticle attractive interactions in this case overcome the electrostatic repulsive forces induced by the KPS fragments. This provides straightforward evidence for the presence of surface

carboxylic acid groups (Figure 2, Panel B). Below the LCST of PNiPAm, all samples are colloidally stable because i) particles are hydrophilic and osmotically swollen, ii) surface pNiPAm chains induce steric repulsion and iii) the surface bears residual charges from initiator fragments. When particles come in close proximity, inter-particle H-bonding in S505 is counterbalanced by the other repulsive terms. Above LCST, the particles are in their deswollen state, driven by the hydrophobic interactions of the isopropyl groups and the expulsion of water from the amides. This happens throughout the volume and on the surface, which means that the steric term is ruled-out and replaced by an attractive term. S304 particles which do not have protonated MAAc on the surface remain stable because the initiator charge is sufficient to counterbalance the interparticle attraction induced by pNiPAm phase separation. S505 still bears surface initiator charge, but in contrast to S304, also bears protonated MAAc on the surface. Aggregation is observed because of the presence of an additional attractive term, beyond that induced by surface phase separated pNiPAm, which is ascribed to interparticle H-bonding. Interparticle hydrophobic interactions between the methyl groups of MAAc are also expected to contribute to the aggregation effect. Moreover, the combined manifestation of a quasi-linear thermal profile at pH=9 and aggregation due to inter-particle attractive interactions, verifies that -COOH groups are distributed throughout the volume of the S505 particles. In order to circumvent the temperature aggregation effect and complete the DLS thermal study at the acidic pH testing conditions, the sample was measured at C_{SDS} = 0.82 mM which is tenfold smaller than the CMC and ensures the absence of SDS micelles inside the microgels network.

S738 exhibited a unique thermal behavior, that suggests a distribution of charge that is distinct from that found in S505 and S304. At pH=9, S738 adopts the typical sigmoidal deswelling profile expected for pristine pNiPAm microgels, with a VPT in the vicinity of 32.5 °C. This picture implies a minor volumetric distribution of charge and a preferential accumulation near the microgel periphery. When heated at pH=4, S738 exhibits a similar aggregation behavior with S505, which was once again alleviated with the addition of SDS (Figure 3, Panel A).

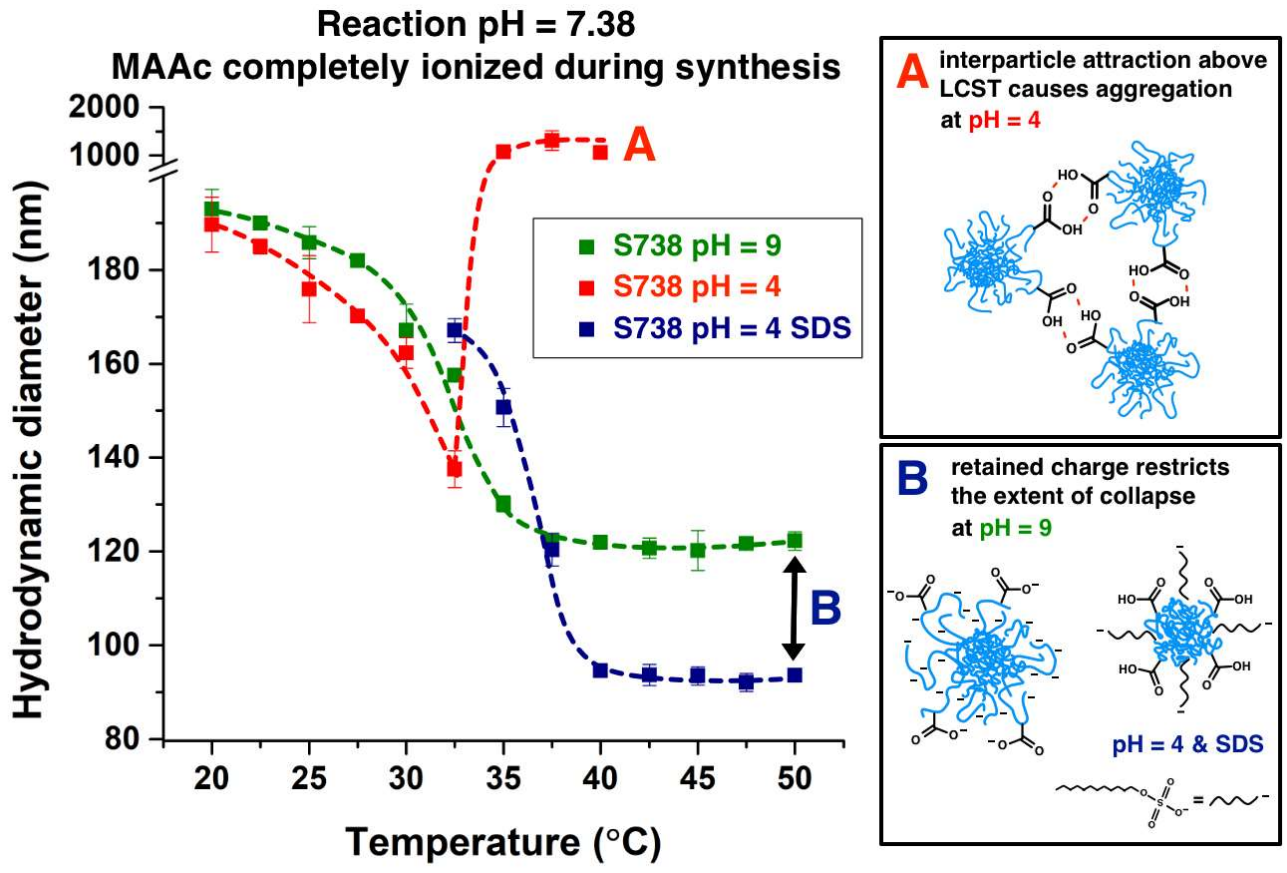

Figure 3. D_h versus T profiles for S738 at pH=4 and pH=9. Dashed lines are visual aids. Panel A: at pH=4 the behavior is similar to S505. Panel B: at pH=9, the charged hairy shell opposes deswelling and a substantial difference in hydrodynamic dimensions is evident between the collapsed states at pH=4 in the presence of SDS.

Although the microgel dimensions is expected to remain unaffected by the presence of SDS at $C_{SDS} << CMC_{SDS}$ [40], a higher size is recorded at 32.5 °C. We ascribe this difference to the shift of the VPT to the right as a result of the adsorption of unimer SDS molecules inside the particle network [41]. A similar but smaller effect is observed for S505. While no pH induced swelling was evident at 20 °C, S738 exhibited a notable difference in size in the collapsed state, between the alkaline and acidic testing conditions (Figure 4, Panel B), which correlates further with the presence of a charged periphery that thwarts particle collapse.

Electron Microscopy Study. While DLS has the advantage of probing particles in their native state, charge distribution information was indirectly inferred through the thermal behavior. On the other extreme, electron microscopy yields information at the individual particle level, and with nanoscale resolution; however, particles are interrogated in the collapsed, dehydrated form. In order to reliably correlate the greyscale intensity in TEM with the local concentration of carboxylic acid groups, some conditions should hold. Firstly, uranyl cations should bind exclusively to MAAc and present negligible

non-specific binding to NiPAm residues. This feature has been demonstrated in the work of Lyon and Jones [42], where only the shell of PNiPAm core/P(NiPAm-co-AAc) shell particles was stained by the heavy metal cations. Secondly, the staining of the MAAc residues should be quantitative, which in our study was ensured by the treatment of the suspensions with an excess of uranyl cations in respect to the acid residues. Furthermore, our particles are spherically symmetric and well-isolated from the background, which facilitates mathematical averaging. It is important to note that relative intensity distributions are calculated and not absolute values. This approach of grayscale analysis of TEM images to quantitatively determine carboxylic acid distributions of uranyl acetate stained P(NiPAm-co-MAAc) microgels has been used previously by Hoare et al. [29]. In order to obtain the volume normalized distribution of charge with respect to normalized dimensions ([-COOH] versus r/r_0) and enable the direct comparison across samples, a clear particle boundary must be defined. We have unambiguously defined r_0 by performing SEM imaging of the same samples used in the TEM study (Figure 4). Finally, we note that isoelectric titrations have been employed in the literature for the investigation of -COOH topology through the dependence of pK_a on the degree of ionization, α, of MAAc, but since conflicting correlative trends were identified for this material system [22],[23] we chose to use direct morphological imaging with TEM.

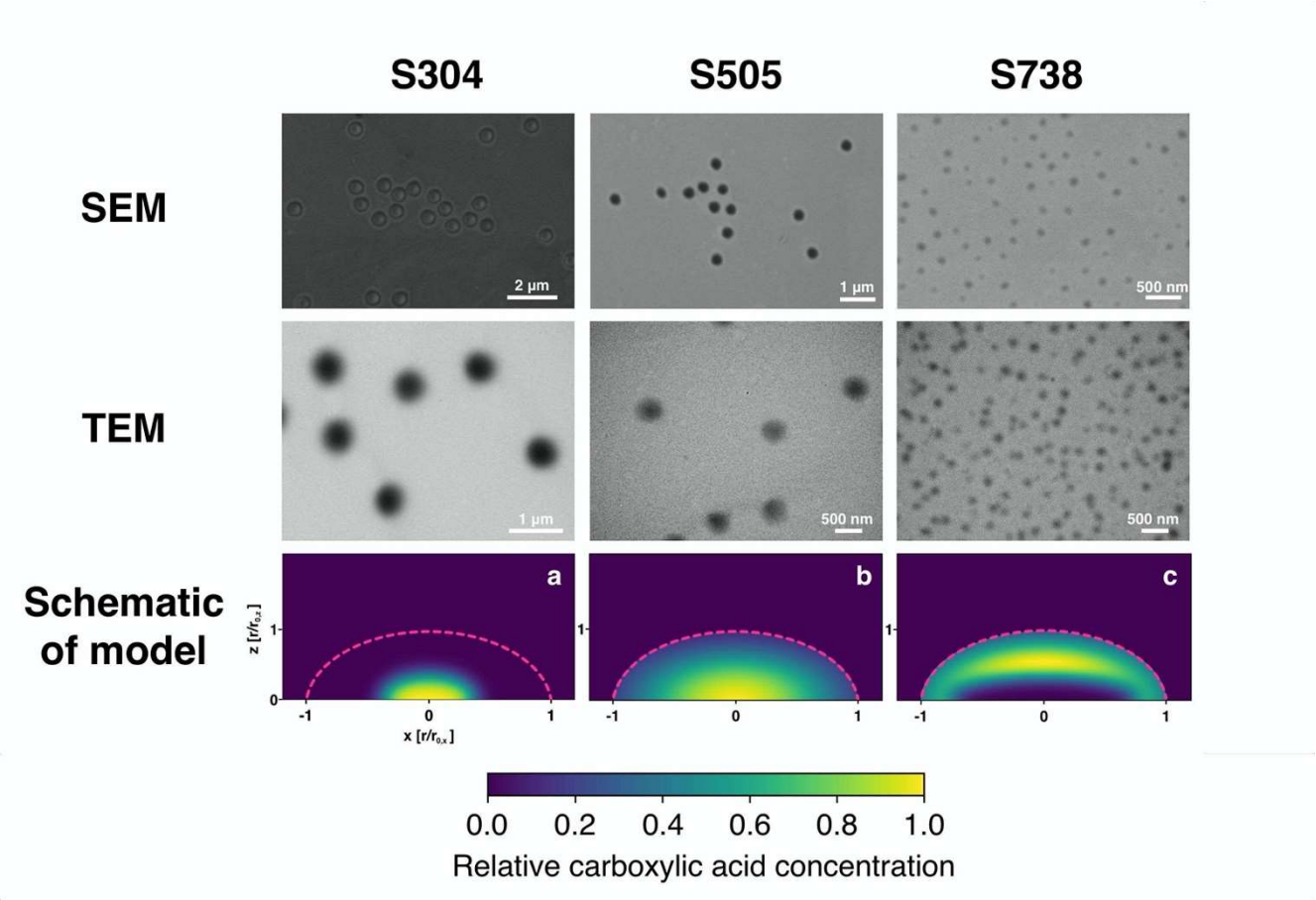

Figure 4. SEM/TEM photomicrographs of samples and XZ cross-sections of the modeled elliptically deformed particles showing distribution of -COOH groups. Yellow color in the schematic of the model denotes high concentration of -COOH groups. Normalized dimensions are shown; particle boundary, r_0, is indicated with pink dashed line.

In the TEM images, contrast arises from uranium atoms bound to the carboxylic acid species; in the case of S304 where MAAc is polymerized faster than NiPAm, only the core is identified. On the other hand, in the SEM images, the brighter (MAAc rich) core is surrounded by a darker (MAAc depleted) shell, allowing for the direct derivation of both the core dimensions and the overall particle dimensions, r_0. In accordance with the DLS results and our hypothesis that slower MAAc kinetics with increasingly alkaline conditions would extend the distribution of -COOH species towards the particle periphery, the overall particle size by TEM and SEM was identical in the cases of S505 and S738.

Further support for the proposed morphologies comes from examining the line profiles of the TEM images. In order interpret the line profiles, deviation from the ideal spherical shape of particles in suspension must be taken into account. The mechanical rigidity of microgels is correlated with the degree of crosslinking and typically pNiPAm microgels with BIS content less than 10% are considered soft. As a result, dehydrated microgels exhibit a substantial shape deformation when cast on solid substrates [43]. SEM imaging at tilted angles (SI Figure 2) reveals deformations that are consistent with the previous

studies. The -COOH group topologies in each sample were extracted by utilizing models that depicted different possible distributions of the -COOH group in the distorted collapsed form as is the situation while performing TEM studies; in all cases, the collapsed microgel was approximated as a semi-spheroid with the minor axis perpendicular to the Formvar substrate. A core distribution, a core-shell distribution and a heterogeneous shell distribution were modeled and the corresponding projected radial distribution profiles were compared with the line profiles obtained from the TEM images to ascertain the -COOH topology in each sample. We note that although the treatment of the collapsed microgel as a semi-spheroid is a first approximation of the intricate particle deformation process on the Formvar substrate, this simple model matches well with the experimental data of the TEM grayscale analysis (Figure 6) and evidently captures the different -COOH group topologies in the samples. The deviations in the curvature of the profiles predicted by the model at the extremes of the microgel can be attributed to the deviation of the semi-spheroid approximation from the "sombrero-like" morphologies captured in the SEM micrographs.

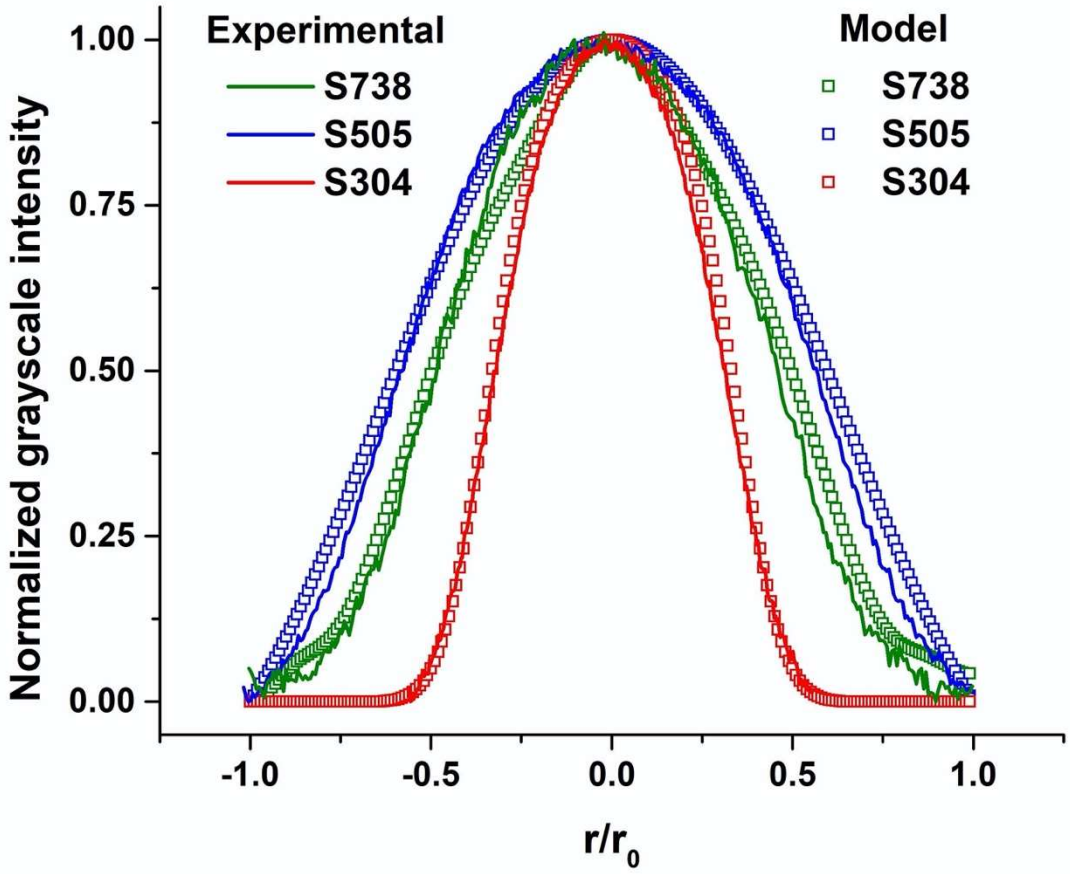

Figure 5. Greyscale analysis of the TEM images is directly correlated with the spatial distribution of -COOH groups. The experimental profiles are in excellent agreement with the predictions of our model which takes into account the effect of particle deformation on the Formvar substrate.

Reaction pH affects size. Final microgel size is governed by the stability of primary nuclei formed in the early stages of polymerization [44]. We have ruled out the likelihood of smaller particle size in increasingly alkaline conditions due to the production of a higher polymer sol fraction since the particle yield is consistent across samples (SI Table 1). We ascribe the size modulation to the inherent surfactant-like nature of the p(NiPAm-co-MAAc) chains with charged substituents at T > LCST. At the polymerization temperature, the growing chains are composed of dissociated $MAAc^{-}Na^{+}$ monomeric units and NiPAm residues bearing isopropyl groups. The coexistence of hydrophobic/hydrophilic species induces surfactant action, which is also qualitatively verified by the intense foaming of the reaction at pH=7.38 if Ar sparging is continued after the 20 sec imposed for monomer mixing. In order to interpret the pH-induced size modulation effect we turned our attention to the established model of SDS size modulation [45]. The analogies with our system are summarized in Figure 6. From a mechanistic viewpoint, i) the growing primary chains form aggregates termed as primary nuclei, ii) these primary nuclei further aggregate to form precursor particles, iii) the accumulation of charge on the surface of precursor particles hinders further aggregation and iv) particles grows by the attachment of oligomers or direct monomer addition. In our case, the growing chains are amphiphilic in nature which translates into precursor particles reaching the critical surface charge to volume ratio for colloidal stability at lower degrees of primary nuclei association. In other words, the final microgel size is smaller because the total monomer content is partitioned in a higher number of precursor particles.

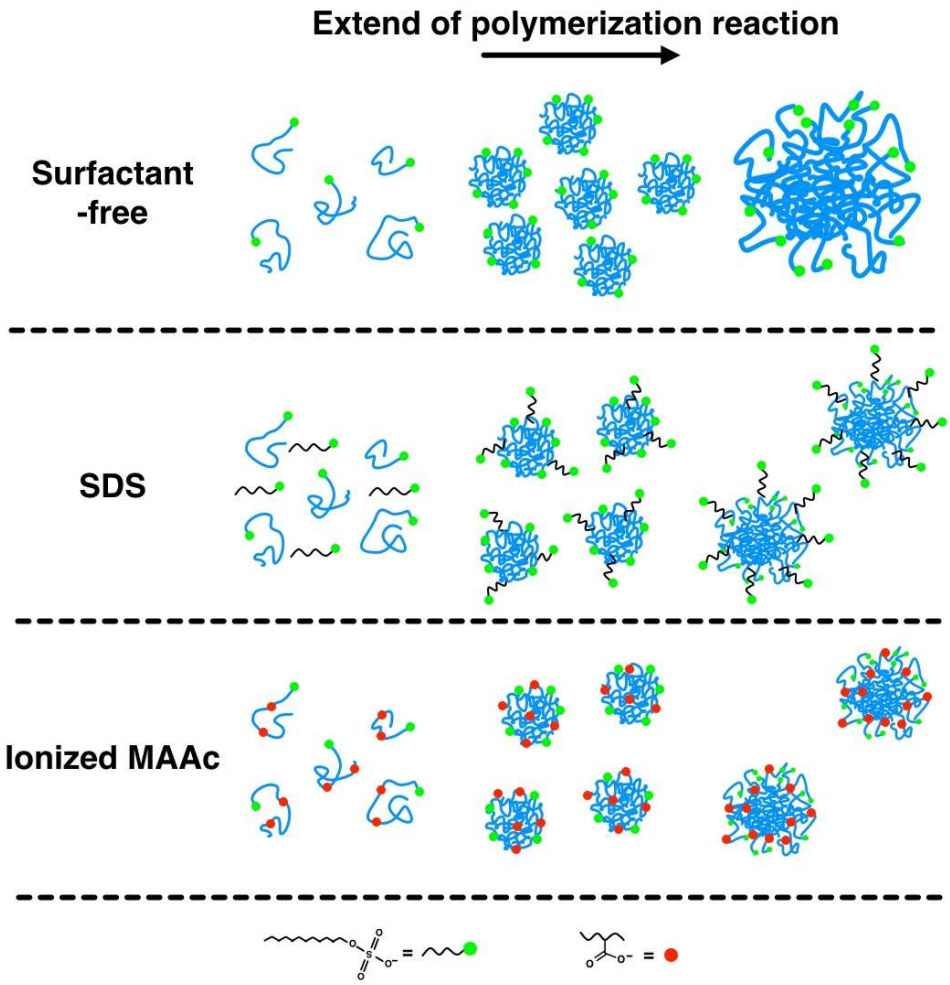

Figure 6. Cartoon of the proposed mechanism of surfactant action.

Reaction pH affects carboxylic acid distribution. The significance of pH as a compositional handle was highlighted in a recent work by Scott *et al.* [46] where they studied a linear terpolymer system consisted of acrylamide, acrylic acid and 2-acrylamido-2-methylpropane sulfonic acid. We postulated that a direct analogy would hold for our microgel terpolymers of NiPAm-BIS-MAAc. At the low polymerization conditions (pH=3.04), MAAc is polymerized faster than NiPAm and tracks more closely the kinetics of BIS leading to a preferential localization to the particles' core. This was independently verified by DLS and electron microscopy and is in line with the literature. At the intermediate reaction pH (pH=5.05) the system is at the regime of the so-called crossover conditions and the reaction is a quaterpolymerization of NiPAm/BIS/MAAc/$MMAc^{-}Na^{+}$. In this case, the uncharged fraction of the MAAc monomer is incorporated towards the particle core as a result of $k_{MAAc} > k_{NiPAm}$. The remaining charged $MAAc^{-}Na^{+}$ will react in the early stages of polymerization at a slower rate than NiPAm (and cause the more effective stabilization of primary nuclei, resulting in $D_{h,S738} < D_{h,S505} < D_{h,S304}$), while the

rest is polymerized at a later stage where the particle has evolved, thus enriching the particle with carboxyl groups towards the shell. The spatial distribution of -COOH can be regulated by pH, as evidenced by the preferential incorporation of charge towards the shell in the case of S738. Finally, we note that the DLS thermal profile of S738 is consistent with a more hairy surface than S505 and S304 due to the faster BIS kinetics in the presence of $MAAc^{-}Na^{+}$ [29].

Conclusions

We have presented a novel one-pot surfactant-free method for the modulation of size and carboxylic acid group distribution in pNiPAm-based thermoresponsive microgels. As an improved alternative to previously reported semi-batch protocols which relied on the use of feeding pumps for the control of microgel physicochemical characteristics [22],[23],[30],[47], we identified reaction pH as a facile process variable which generates equivalent modulation of charge distribution. Our hypothesis of pH controlled charge distribution was based on three concepts: i) the dependence of kinetic reactivity of MAAc on the degree of ionization [26], ii) the modulation of the degree of 'blockiness' of linear MAAc copolymers by reaction pH [27] and iii) the manifestation of solution polymerization kinetics in precipitation polymerization, suggesting that linear chains grow in the continuous phase prior attachment to the dispersed phase [28]. We examined three cases of reaction conditions at pH = 3.04, pH = 5.05 and pH =7.38, corresponding to fully protonated, partially dissociated and fully ionized forms of the MAAc monomer, respectively. Specifically, we validated the hypothesis that the relative reactivity difference of these monomer forms with the main monomer NiPAm resulted in the tailoring of three different charge topologies, namely core-localized (S304), homogeneous (S505) and shell-localized (S738). Additionally, a size modulation effect ($D_{h,S304} > D_{h,S505} > D_{h,S738}$) was observed. We rationalized that the monotonically increasing surfactant character of the growing p(NiPAm-*co*-MAAc) chains as a function of reaction pH correlates with a gradually more effective stabilization of primary nuclei which explains the size trend.

We combined DLS with SEM/TEM for the characterization of the colloids and developed a mathematical model for the interpretation of the TEM greyscale data. The microgel deswelling profiles and colloidal stability, as tested in alkaline and acidic conditions, served as strong indicators of the underlying charge topologies, which were substantiated by TEM greyscale image analysis of uranyl acetate stained microgels. Building on a quantitative relationship between signal intensity and local functional group concentration through electron and super resolution microscopy of microgel colloids that has been previously established in the literature [22],[29],[48],[49],[50], we developed a simple

protocol whereby 2D images extracted with the established techniques are used for the estimation of 3D spatial information. Assuming a semi-spheroid as a first-approximation for the observed "sombrero-like" morphology, our model captures the underlying charge distributions while accounting for drying induced distortions. We anticipate the methodology developed here for the extraction of quantitative information from greyscale analysis, will find utility in similar systems which are known to be affected by deformation during the measurement conditions. Lastly, we are exploring the scalability of our one-pot, non-stirred and single-process variable method for multi-gram batches of functional soft colloids.

Conflicts of interest

There are no conflicts to declare.

Acknowledgements

This work is based in part upon work supported by the National Science Foundation under grant no. 1654599 and American Chemical Society Petroleum Research Foundation under grant no. 56823DNI7. We thank Prof. Helen Zha and Prof. Edmund Palermo for graciously allowing use of their laboratory facilities. RPI staff at the CBIS Proteomics and Analytical Biochemistry Cores are acknowledged for facilitating part of the experimental work.

Bibliography

[1] Wu Q, Su T, Mao Y, Wang Q. Thermal responsive microgels as recyclable carriers to immobilize active proteins with enhanced nonaqueous biocatalytic performance. Chem Commun 2013;49:11299. https://doi.org/10.1039/c3cc46161k.

[2] Dubey NC, Tripathi BP, Müller M, Stamm M, Ionov L. Enhanced Activity of Acetyl CoA Synthetase Adsorbed on Smart Microgel: an Implication for Precursor Biosynthesis. ACS Appl Mater Interfaces 2015;7:1500–7. https://doi.org/10.1021/am5063376.

[3] Zhang et al. - 2014 - Optical Devices Constructed from Multiresponsive M.pdf n.d.

[4] Contreras-Cáceres R, Pastoriza-Santos I, Alvarez-Puebla RA, Pérez-Juste J, Fernández-Barbero A, Liz-Marzán LM. Growing Au/Ag Nanoparticles within Microgel Colloids for Improved Surface-Enhanced Raman Scattering Detection. Chemistry – A European Journal 2010;16:9462–7. https://doi.org/10.1002/chem.201001261.

[5] Kwok M, Ambreen J, Ngai T. Correlating the effect of co-monomer content with responsiveness and interfacial activity of soft particles with stability of corresponding smart emulsions. Journal of Colloid and Interface Science 2019;546:293–302. https://doi.org/10.1016/j.jcis.2019.03.072.

[6] Suzuki D, Kobayashi T, Yoshida R, Hirai T. Soft actuators of organized self-oscillating microgels. Soft Matter 2012;8:11447. https://doi.org/10.1039/c2sm26477c.

[7] Serpe MJ, Yarmey KA, Nolan CM, Lyon LA. Doxorubicin Uptake and Release from Microgel Thin Films. Biomacromolecules 2005;6:408–13. https://doi.org/10.1021/bm049455x.

[8] Das M, Mardyani S, Chan WCW, Kumacheva E. Biofunctionalized pH-Responsive Microgels for Cancer Cell Targeting: Rational Design. Adv Mater 2006;18:80–3. https://doi.org/10.1002/adma.200501043.

[9] Karg M, Pich A, Hellweg T, Hoare T, Lyon LA, Crassous JJ, et al. Nanogels and Microgels: From Model Colloids to Applications, Recent Developments, and Future Trends. Langmuir 2019;35:6231–55. https://doi.org/10.1021/acs.langmuir.8b04304.
[10] Agrawal G, Agrawal R. Functional Microgels: Recent Advances in Their Biomedical Applications. Small 2018;14:1801724. https://doi.org/10.1002/smll.201801724.
[11] Arleth L, Xia X, Hjelm RP, Wu J, Hu Z. Volume transition and internal structures of small poly(*N* -isopropylacrylamide) microgels. J Polym Sci B Polym Phys 2005;43:849–60. https://doi.org/10.1002/polb.20375.
[12] Pelton R. Poly(N-isopropylacrylamide) (PNIPAM) is never hydrophobic. Journal of Colloid and Interface Science 2010;348:673–4. https://doi.org/10.1016/j.jcis.2010.05.034.
[13] Hoare T, Pelton R. Highly pH and Temperature Responsive Microgels Functionalized with Vinylacetic Acid. Macromolecules 2004;37:2544–50. https://doi.org/10.1021/ma035658m.
[14] Yin J, Hu H, Wu Y, Liu S. Thermo- and light-regulated fluorescence resonance energy transfer processes within dually responsive microgels. Polym Chem 2011;2:363–71. https://doi.org/10.1039/C0PY00254B.
[15] Zhang QM, Wang W, Su Y-Q, Hensen EJM, Serpe MJ. Biological Imaging and Sensing with Multiresponsive Microgels. Chem Mater 2016;28:259–65. https://doi.org/10.1021/acs.chemmater.5b04028.
[16] Hoare T, Pelton R. Charge-Switching, Amphoteric Glucose-Responsive Microgels with Physiological Swelling Activity. Biomacromolecules 2008;9:733–40. https://doi.org/10.1021/bm701203r.
[17] Hoare T, Pelton R. Impact of Microgel Morphology on Functionalized Microgel−Drug Interactions. Langmuir 2008;24:1005–12. https://doi.org/10.1021/la7024507.
[18] Scheidegger L, Fernández-Rodríguez MÁ, Geisel K, Zanini M, Elnathan R, Richtering W, et al. Compression and deposition of microgel monolayers from fluid interfaces: particle size effects on interface microstructure and nanolithography. Phys Chem Chem Phys 2017;19:8671–80. https://doi.org/10.1039/C6CP07896F.
[19] Hoare T, Young S, Lawlor MW, Kohane DS. Thermoresponsive nanogels for prolonged duration local anesthesia. Acta Biomaterialia 2012;8:3596–605. https://doi.org/10.1016/j.actbio.2012.06.013.
[20] Lindman S, Lynch I, Thulin E, Nilsson H, Dawson KA, Linse S. Systematic Investigation of the Thermodynamics of HSA Adsorption to N-iso-Propylacrylamide/N-tert-Butylacrylamide Copolymer Nanoparticles. Effects of Particle Size and Hydrophobicity. Nano Lett 2007;7:914–20. https://doi.org/10.1021/nl062743+.
[21] Hoare T, Pelton R. Characterizing charge and crosslinker distributions in polyelectrolyte microgels. Current Opinion in Colloid & Interface Science 2008;13:413–28. https://doi.org/10.1016/j.cocis.2008.03.004.
[22] Sheikholeslami P, Ewaschuk CM, Ahmed SU, Greenlay BA, Hoare T. Semi-batch control over functional group distributions in thermoresponsive microgels. Colloid Polym Sci 2012;290:1181–92. https://doi.org/10.1007/s00396-012-2642-x.
[23] Wei J, Li Y, Ngai T. Tailor-made microgel particles: Synthesis and characterization. Colloids and Surfaces A: Physicochemical and Engineering Aspects 2016;489:122–7. https://doi.org/10.1016/j.colsurfa.2015.10.042.
[24] Zhou S, Chu B. Synthesis and Volume Phase Transition of Poly(methacrylic acid- *co* - *N* -isopropylacrylamide) Microgel Particles in Water. J Phys Chem B 1998;102:1364–71. https://doi.org/10.1021/jp972990p.
[25] Rintoul I, Wandrey C. Polymerization of ionic monomers in polar solvents: kinetics and mechanism of the free radical copolymerization of acrylamide/acrylic acid. Polymer 2005;46:4525–32. https://doi.org/10.1016/j.polymer.2005.04.005.
[26] Lacík I, Učňová L, Kukučková S, Buback M, Hesse P, Beuermann S. Propagation Rate Coefficient of Free-Radical Polymerization of Partially and Fully Ionized Methacrylic Acid in Aqueous Solution. Macromolecules 2009;42:7753–61. https://doi.org/10.1021/ma9013516.
[27] Dubey A, Burke NAD, Stöver HDH. Preparation and characterization of narrow compositional distribution polyampholytes as potential biomaterials: Copolymers of *N* -(3-aminopropyl)methacrylamide hydrochloride (APM) and methacrylic acid (MAA). J Polym Sci Part A: Polym Chem 2015;53:353–65. https://doi.org/10.1002/pola.27377.
[28] Virtanen OLJ, Richtering W. Kinetics and particle size control in non-stirred precipitation polymerization of N-isopropylacrylamide. Colloid Polym Sci 2014;292:1743–56. https://doi.org/10.1007/s00396-014-3208-x.

[29] Hoare T, McLean D. Kinetic Prediction of Functional Group Distributions in Thermosensitive Microgels. J Phys Chem B 2006;110:20327–36. https://doi.org/10.1021/jp0643451.
[30] Acciaro R, Gilányi T, Varga I. Preparation of Monodisperse Poly(*N* -isopropylacrylamide) Microgel Particles with Homogenous Cross-Link Density Distribution. Langmuir 2011;27:7917–25. https://doi.org/10.1021/la2010387.
[31] Karanastasis AA, Kenath GS, Sundararaman R, Ullal CK. Quantification of functional crosslinker reaction kinetics *via* super-resolution microscopy of swollen microgels. Soft Matter 2019;15:9336–42. https://doi.org/10.1039/C9SM01618J.
[32] Smith MH, Herman ES, Lyon LA. Network Deconstruction Reveals Network Structure in Responsive Microgels. J Phys Chem B 2011;115:3761–4. https://doi.org/10.1021/jp111634k.
[33] Hoare T, Pelton R. Functional Group Distributions in Carboxylic Acid Containing Poly(*N* -isopropylacrylamide) Microgels. Langmuir 2004;20:2123–33. https://doi.org/10.1021/la0351562.
[34] Kratz K, Hellweg T, Eimer W. Influence of charge density on the swelling of colloidal poly(N-isopropylacrylamide-co-acrylic acid) microgels. Colloids and Surfaces A: Physicochemical and Engineering Aspects 2000;170:137–49. https://doi.org/10.1016/S0927-7757(00)00490-8.
[35] Burmistrova A, Richter M, Eisele M, Üzüm C, Von Klitzing R. The Effect of Co-Monomer Content on the Swelling/Shrinking and Mechanical Behaviour of Individually Adsorbed PNIPAM Microgel Particles. Polymers 2011;3. https://doi.org/10.3390/polym3041575.
[36] Sun W, An Z, Wu P. Hydrogen bonding reinforcement as a strategy to improve upper critical solution temperature of poly(*N* -acryloylglycinamide- *co* -methacrylic acid). Polym Chem 2018;9:3667–73. https://doi.org/10.1039/C8PY00733K.
[37] Pelton RH, Chibante P. Preparation of aqueous latices with N-isopropylacrylamide. Colloids and Surfaces 1986;20:247–56. https://doi.org/10.1016/0166-6622(86)80274-8.
[38] Tagit O, Tomczak N, Vancso GJ. Probing the Morphology and Nanoscale Mechanics of Single Poly(N-isopropylacrylamide) Microgels Across the Lower-Critical-Solution Temperature by Atomic Force Microscopy. Small 2008;4:119–26. https://doi.org/10.1002/smll.200700260.
[39] Zeiser M, Freudensprung I, Hellweg T. Linearly thermoresponsive core–shell microgels: Towards a new class of nanoactuators. Polymer 2012;53:6096–101. https://doi.org/10.1016/j.polymer.2012.10.001.
[40] Woodward NC, Chowdhry BZ, Leharne SA, Snowden MJ. The interaction of sodium dodecyl sulphate with colloidal microgel particles. European Polymer Journal 2000;36:1355–64. https://doi.org/10.1016/S0014-3057(99)00207-4.
[41] Tam KC, Ragaram S, Pelton RH. Interaction of Surfactants with Poly(N-isopropylacrylamide) Microgel Latexes. Langmuir 1994;10:418–22. https://doi.org/10.1021/la00014a015.
[42] Jones CD, Lyon LA. Synthesis and Characterization of Multiresponsive Core−Shell Microgels. Macromolecules 2000;33:8301–6. https://doi.org/10.1021/ma001398m.
[43] Horecha M, Senkovskyy V, Synytska A, Stamm M, Chervanyov AI, Kiriy A. Ordered surface structures from PNIPAM-based loosely packed microgel particles. Soft Matter 2010;6:5980. https://doi.org/10.1039/c0sm00634c.
[44] Pelton R, Hoare T. Microgels and Their Synthesis: An Introduction. Wiley Online Library 2011. https://onlinelibrary.wiley.com/doi/abs/10.1002/9783527632992.ch1 (accessed November 19, 2019).
[45] McPhee W, Tam KC, Pelton R. Poly(N-isopropylacrylamide) Latices Prepared with Sodium Dodecyl Sulfate. Journal of Colloid and Interface Science 1993;156:24–30. https://doi.org/10.1006/jcis.1993.1075.
[46] Scott AJ, Duever TA, Penlidis A. The role of pH, ionic strength and monomer concentration on the terpolymerization of 2-acrylamido-2-methylpropane sulfonic acid, acrylamide and acrylic acid. Polymer 2019;177:214–30. https://doi.org/10.1016/j.polymer.2019.06.006.
[47] Kardos A, Gilányi T, Varga I. How small can poly(N-isopropylacrylamide) nanogels be prepared by controlling the size with surfactant? Journal of Colloid and Interface Science 2019;557:793–806. https://doi.org/10.1016/j.jcis.2019.09.053.
[48] Bergmann S, Wrede O, Huser T, Hellweg T. Super-resolution optical microscopy resolves network morphology of smart colloidal microgels. Phys Chem Chem Phys 2018;20:5074–83. https://doi.org/10.1039/C7CP07648G.

[49] Otto P, Bergmann S, Sandmeyer A, Dirksen M, Wrede O, Hellweg T, et al. Resolving the internal morphology of core–shell microgels with super-resolution fluorescence microscopy. Nanoscale Adv 2020;2:323–31. https://doi.org/10.1039/C9NA00670B.
[50] Karanastasis AA, Zhang Y, Kenath GS, Lessard MD, Bewersdorf J, Ullal CK. 3D mapping of nanoscale crosslink heterogeneities in microgels. Mater Horiz 2018;5:1130–6. https://doi.org/10.1039/C8MH00644J.